TRI-PP-79-35
TRI-UAE-5021
Sep 1979

Proton-^{4}He elastic scattering at intermediate energies

G.A. Moss, L.G. Greeniaus, J.M. Cameron, D.A. Hutcheon,
R.L. Liljestrand, C.A. Miller, and G. Roy
Department of Physics, The University of Alberta, Edmonton, Canada T6G 2N5

B.K.S. Koene* and W.T.H. van Oers
Department of Physics, The University of Manitoba, Winnipeg, Canada R3T 2N2

A.W. Stetz
Department of Physics, Oregon State University, Corvallis, Oregon 97331

A. Willis and N. Willis
Institut de Physique Nucléaire, 91406 Orsay, France

Abstract

The differential cross section and analyzing power for p-^{4}He elastic scattering at 200, 350, and 500 MeV incident proton energy in the laboratory angle range from 4° to 168° are presented. Comparisons to theoretical calculations at 200 and 350 MeV have been made.

(submitted to Physical Review C)

I. INTRODUCTION

Proton-nucleus scattering at intermediate energies has received considerable attention with the advent of accelerators capable of producing high-intensity, variable-energy polarized beams with good energy resolution. Extensive data for differential cross sections and analyzing powers have been obtained, which should provide a stimulus to the search for a successful microscopic description of the processes involved.

The elastic scattering of protons from ^{4}He is an unusually good case to investigate thoroughly for several reasons: the initial and final states are well defined theoretically; the target nucleus has spin zero, minimizing the complications that arise in some spin-dependent calculations; and inelastic processes are easily distinguishable, which reduces experimental demands on energy resolution.

It has become apparent that analyzing power (polarization) angular distributions are very important in the evaluation of the validity of theoretical models. In the energy range of the present experiment, 200 to 500 MeV, the analyzing power exhibits a rich and variable structure. Although a proper description of the differential cross section has established the need for spin-dependent terms, far more stringent demands are established when analyzing power data are to be explained as well.

The present experiment represents the last phase of a three-part study of p-^{4}He elastic scattering at TRIUMF. The first part[1] examined $d\sigma(\theta)/d\Omega$ and $A_y(\theta)$ in the small-angle region (4°-16° in the laboratory). This measurement was made with a gas target which had a well-defined density and thickness. The cross section results of this first phase have been used as a normalization benchmark for the remaining two parts of the study.

The second part of the investigation[2] involved measurement of $d\sigma(\theta)/d\Omega$ and $A_y(\theta)$ at backward angles (144°-168° in the laboratory) for several incident proton energies between 185 and 500 MeV. One of the goals of the experiment was a careful search for energy-dependent backward peaking of the differential cross section. The analyzing power measurements made at the same time were intended to aid in a more complete understanding of the reaction process.

In the present experiment we have completed the cross section and

analyzing power angular distributions at 200, 350, and 500 MeV with measurements in the intermediate-angle region. At these three energies, data sets spanning the laboratory angle range from 4° to 168° are now available.

Section II of this report discusses the experiment while Sec. III describes the analysis procedures. Results and discussion are presented in Sec. IV and conclusions are summarized in Sec. V.

II. THE EXPERIMENT

The experiment was performed using the external 4B proton beam line at the TRIUMF cyclotron. Most of the features of the apparatus have been described elsewhere[1-3] so that only aspects specific to the present experiment will be discussed in detail.

The target-detector apparatus is represented schematically in Fig. 1(a) and 1(b). Some important characteristics of the system are also summarized in Table I. The liquid ^{4}He target[4,5] had a thickness of 0.77 cm (97 mg/cm^2) with a 5 cm^2 aperture. The target cell could be raised and lowered remotely. This permitted the normal ^{4}He cell to be replaced in the beam by an empty target cell of equivalent thickness in order to correct for background coming from material around the liquid ^{4}He. The target could also be rotated to ensure that none of the scattered particles would strike the side frames of the cell. The scattered particles were detected in counter telescopes consisting of 12.5 cm^2 multiwire proportional chambers (MWPC) with horizontal and vertical coordinates, plastic scintillation detectors, copper energy degraders, and NaI (Tℓ) detectors. The telescopes were mounted on four independently movable booms which could be remotely positioned about the target centre to an accuracy of 0.1°. The efficiencies of the telescopes have been carefully measured[6] so that proper corrections for losses due to nuclear interactions in the copper and NaI could be made.

Two modes of operation were employed: a singles mode shown in Fig. 1(a) when only the scattered proton could be detected, and a coincidence set-up as shown in Fig. 1(b) when the ^{4}He recoil could be detected in coincidence with the proton. Events with protons scattered to the left and to the right of the beam could be detected if the paths of the scattered particles were not obscured by the target frames. Both 'left'

and 'right' events were collected concurrently when the target geometry permitted. A 'left' or 'right' event was always defined by the side to which the proton was scattered. In the angular range from 60° to 120° events were detected on only one side of the beam.

In the coincidence mode, the proton was detected in one of the back detector telescopes while the recoil ^{4}He was detected in the forward telescope on the opposite side of the beam. A trigger ($\Delta E_F \cdot E_B \cdot \Delta E_B$) was required to define an event. The copper degrader thickness in the back telescopes was varied depending on the energy of the scattered protons so as to keep the proton energy at the entrance to the NaI detector in the range between 80 and 130 MeV. The coincidence mode gave excellent discrimination in the selection of elastic events so that the data were essentially free of any background.

The singles mode was used when the recoil ^{4}He did not have sufficient energy to penetrate the target and the material before the ΔE detectors. In this case the protons were detected in the front telescopes, the trigger defining the event being ($P \cdot \Delta E_F \cdot E_F$). Here an additional counter (P) was placed about 50 cm from the target and operated in coincidence with the other counters in the telescope. It served as an active collimator to eliminate protons that did not scatter from the immediate region of the liquid ^{4}He target. Again copper degraders were used to limit the proton energy in the NaI detectors. Data collected in the singles mode were composed of p-^{4}He elastic and inelastic scattering events, and background events from the target walls and thermal insulation.

The calculated rms multiple scattering of the protons in singles mode was always less than 0.3 degrees, and effects on the measured differential cross sections have been ignored. In the coincidence mode, the distribution of recoil ^{4}He particles was observed with the FL and FR wire chambers; the cuts on the proton solid angle were chosen so that losses due to multiple scattering of the recoil particles were negligible.

A polarized proton beam was used for all measurements. The beam intensities ranged from 0.2 to 10 nA with typical polarizations between 65% and 75%. The polarization direction, which could be reversed at the ion source, could also be set to zero to provide unpolarized beam for control purposes. The beam spot size on target was approximately 0.5 cm in diameter; its position was monitored regularly by observing the spot on a

scintillator at the target station and by removable beam line wire scanners upstream and downstream of the target. The polarization of the beam was monitored continuously during data collection by a polarimeter[3] upstream of the ^{4}He target. The polarization was determined from the asymmetry in proton-proton scattering from a thin, 5 mg/cm^2, CH_2 target. The statistical uncertainty in the determination of the beam polarization during a given run was less than 1%. Corrections due to contributions from the carbon in the target were made as discussed in Ref. 3.

Data acquisition was accomplished via a CAMAC system interfaced to a Honeywell 316 computer. Data were recorded event by event on magnetic tape with 'left' and 'right' events appropriately identified. The acquisition program also allowed a rudimentary analysis of the data to be made on line so that their quality could be checked.

Two independent beam flux monitors were used to provide an independent determination of the absolute scale of the cross sections and to permit the correct combination of data collected with different beam polarizations. These monitors were (1) the beam polarimeter, where the number of p-p elastic scattering events was monitored throughout each run, and (2) an ionization chamber situated downstream of the helium target. Both the polarimeter target foil and the ionization chamber had been previously calibrated at each energy by using a Faraday cup installed in the beam line. Although these monitors were used only for relative normalizations, the values of the cross sections extracted by using them agreed with those of Ref. 1 to better than 10% in all cases. The final data presented here were normalized to the results of Ref. 1 in the regions of angle overlap.

III. ANALYSIS PROCEDURES

Data collected in the two modes of operation were treated separately in the off-line analysis. For the singles data, horizontal and vertical MWPC cuts were made to select only those events in the central region of the NaI detector where the detection efficiency was uniform (see Table I). A representative spectrum at a proton energy of 500 MeV is shown in Fig. 2(a). The spectrum after the background from the target walls has been subtracted is also presented. The two arrows in the figure show the final cuts around the well-defined elastic scattering peak. In the cross

section calculation, corrections were made for events lost due to wire chamber inefficiencies (about 6%), for nuclear interactions of the protons while stopping in the total energy telescope,[6] and for the dead-time of the system. The interaction correction was dependent on the mean energy incident on the telescope and varied between 10% and 70% depending on the beam energy and the angle setting. Uncertainties in this correction are 0.5-1.5%.[6]

The dead-time of the system was dominated by the computer data acquisition and the on-line calculations. Dead-time corrections were calculated in two ways. The ratio of events detected in the electronics and the number actually accepted and written on magnetic tape was used in the final analysis. Artificial 'events' created using a pulser and light-emitting diodes on each of the detectors showed that the electronic dead-times were totally negligible in the experiment. The size of the dead-time correction was dependent on the beam flux, with typical values being about 15%. In several cases, data were collected at a given angle and beam polarization orientation but with different beam flux in order to check for possible systematic effects when dead-time corrections were large. Even in cases where the dead-time adjustment was larger than a factor 2, excellent agreement was obtained with cross sections from data with more typical corrections.

The compensation for the wire chamber efficiencies was determined by observing the events corresponding to the elastic proton peak in the NaI spectra, and then finding the fraction of events that had any combination of multiple tracks or misses in the individual coordinate planes used to define the trajectory of the particle. Since the areas of the NaI detectors were smaller than those of the wire chamber, this provided a good estimate of inefficiencies in the region of interest. Losses were typically around 4% due to multiple tracks and around 2% for misses.

In the coincidence mode, the correlation of the proton energy in the NaI detector with the energy deposited in the ΔE counter by the associated ^{4}He recoil allowed the desired events to be identified unambiguously. An example is shown in Fig. 2(b). With the addition of time-of-flight cuts, all background was eliminated from this type of data. The wire chambers in the FL and FR telescopes were used only to verify that all the ^{4}He recoils were well within the limits of the ΔE counter. Corrections

for proton MWPC efficiencies, system dead-time, and nuclear interactions in the counter telescopes were made in a manner similar to those for the singles data.

In coincidence or singles mode, when both 'left' and 'right' events were observed, the background-corrected differential cross sections were calculated independently for each side (σ_L and σ_R). The differential cross section for an unpolarized beam was then found by taking the simple average,

$$\sigma_0 = \frac{\sigma_L + \sigma_R}{2} . \qquad (1)$$

Similar values were available for polarization up (+), polarization down (-), and for the unpolarized beam. The final result at a given angle was taken as the weighted average of the results for the different beam polarizations. The individual statistical errors were used as the weighting factors. The analyzing power was calculated from

$$A_y(\theta) = \frac{\sigma_L^+ + \sigma_R^- - \sigma_L^- - \sigma_R^+}{\sigma_L^+ + \sigma_R^+ + \sigma_L^- + \sigma_R^-} \cdot \frac{2}{(P^+ + P^-)} , \qquad (2)$$

where the superscripts denote the direction of the beam polarization. Any instrumental asymmetries cancel to first order using this expression.

When events were detected on only one side of the beam (left in this example), more care had to be taken in extracting the equivalent unpolarized cross sections. Writing the observed cross sections with polarization up and down as

$$\sigma_L^+ = \sigma_0(1 + P^+ A_y) \qquad (3)$$

and

$$\sigma_L^- = \sigma_0(1 - P^- A_y) \qquad (4)$$

one obtains for the unpolarized cross section

$$\sigma_0 = \frac{1}{2}\left(\sigma_L^+ + \sigma_L^- - (\sigma_L^+ - \sigma_L^-)\frac{P^+ - P^-}{P^+ + P^-}\right) . \qquad (5)$$

Here P^+ and P^- are the magnitudes of the incident beam polarization for spin up and spin down, and A_y is the analyzing power of the target at the angle being considered.

The analyzing power at the same angle is calculated from the expression

$$A_y(\theta) = \frac{\sigma_L^+ - \sigma_L^-}{\sigma_0(P^+ + P^-)} , \qquad (6)$$

which can be also be written as

$$A_y(\theta) = \frac{\sigma_L^+ - \sigma_L^-}{P^+\sigma_L^- + P^-\sigma_L^+} . \qquad (7)$$

Instrumental asymmetries cancel in this case only if they remain constant for the spin up and spin down measurements. Particular care was taken to ensure that the beam position did not change.

IV. RESULTS AND DISCUSSION

The results of this experiment are presented in Table II and shown in Figs. 3 and 4. In addition, we have included in the tabulation the data from Stetz *et al.*[1] averaged over the same angular acceptance as the present experiment, and the data from McCamis *et al.*[2] which were obtained under very similar conditions to those used here. Figure 3 shows the complete angular distributions for $d\sigma/dt$ at all three energies. The data from the present experiment have been normalized to the results of Ref. 1 in the angular range near 13°-15°. The normalization uncertainty in the data of Stetz *et al.* was 5% and the combined additional statistical uncertainty in the region of overlap of the two experiments is 2%. Almost the entire allowed range of four-momentum transfer -t has been covered at each energy in the combined data from the three measurements.

At 500 MeV the cross section has the expected behaviour with a minimum at $-t = 0.28$ (GeV/c)^2. A quantitative comparison can be made with the results of Klem *et al.*[7,8] at 560 MeV, except in the region of the first minimum and secondary maximum where strong energy dependence in the magnitude of the cross section is known to exist.[8] The average difference between our results at 500 MeV and the data of Klem is 7.4%. For our data, the ratio of the magnitude of the differential cross section at the second maximum to that at the minimum is 1.26, which is consistent with the energy dependence obtained from other experiments.[8] There is a noticeable change in the slope of the cross section around $-t =$ 1.0 (GeV/c)^2, the region where one expects to observe the onset of the triple scattering contribution in a simple Glauber model.

The results at 350 MeV are in agreement with the previous data of Aslanides *et al.*[9] where there is overlap in the angular ranges. In the

overlap region the average difference between the data of the two experiments is 6.8%, which is within the range of the estimated normalization uncertainties. There is, as well, no systematic difference in the shape of the cross sections. The minimum seen at 500 MeV is replaced at 350 MeV by a 'shoulder' at $-t = 0.32$ $(GeV/c)^2$ and again a change in slope occurs at larger values of $-t$, this time around $-t = 1.2$ $(GeV/c)^2$.

The 200 MeV data show a smooth decrease as a function of $-t$ with a small 'shoulder' near $-t = 0.45$ $(GeV/c)^2$ except at large values of $-t$ where there is an abrupt rise. The agreement with the unpublished results of Gotow[10] is not as good as the comparisons at 350 and 500 MeV.

The analyzing power results are illustrated in Fig. 4. Once again, the angular distributions include the data from Refs. 1 and 2. Their values have been adjusted slightly as indicated in Table II by using more recent values of the p-p analyzing powers.[11,12] The uncertainty in the normalization of the analyzing power at each energy is dominated by the uncertainty in the value of the p-p analyzing power used (1.0-1.5%) and the systematic error introduced by the carbon background subtraction in the beam polarimeter (0.5%). Unlike data at energies below 100 MeV,[13] a great deal of structure is apparent in the present data over the whole angular range. A variation from +1.0 to -1.0 in an angle change of only 30° is seen at 200 MeV. In fact our data at this energy yield extrema that are slightly larger in magnitude than 1.0 (although within errors), indicating that the phase-shift predictions of the p-p analyzing power may be slightly high. A second large negative excursion in the analyzing power is also observed at $-t = 0.85$ $(GeV/c)^2$ (see Table II). As the incident energy is increased over 200 MeV the extrema of the analyzing powers are reduced but additional oscillations in A_y appear.

The trend of smaller magnitudes in the oscillations of $A_y(\theta)$ which is seen as one proceeds from 200 to 500 MeV in the present experiment is continued at higher energies.[7] While one finds large positive and negative excursions in the analyzing power at 200 MeV, as the energy increases the minima fill in and the structure smooths out. This behaviour is presented in Fig. 5 where the values of the analyzing power at the first maximum and the first minimum are plotted against incident proton energy. It is of interest to try to understand this behaviour inasmuch as it may

be a manifestation of the phase differences between the spin-dependent and the spin-independent amplitudes used in multiple scattering models.

Figure 6 is a contour diagram of the analyzing power as a function of incident proton energy from 130 to 1800 MeV. The vertical lines are located at the energies and angles where data exist. The contours are drawn in a manner which assumes a systematic behaviour as the energy changes. The increase in structure in the analyzing power as the energy increases is once again illustrated here. An unusual structure in $A_y(\theta)$ can be observed at large angles between 200 and 500 MeV. One should note that in this energy and angle domain there is no backward peaking in the differential cross section,[2] in contrast with the behaviour at both higher and lower energies.

V. CONCLUSIONS

Generally, existing theoretical calculations have been of two types: Glauber multiple scattering theory predictions or optical potential model calculations (see Ref. 14 for a summary). The Glauber model (and extensions thereto) is reasonably successful in describing proton-nucleus scattering at small angles with some differences between experiment and theory appearing at large scattering angles and near diffraction minima. Optical model calculations based on the procedures of Kerman, McManus, and Thaler[15] have been limited by the inexact knowledge of the nucleon-nucleon interaction. Relativistic treatments of the optical model potential based on the Dirac equation such as those of Arnold, Clark, and Mercer[16] have investigated the possibility of achieving a successful systematic description of the experimental data, including polarization results, over a wide energy range.

We have compared our results at 200 MeV and 350 MeV with two different calculations. At 200 MeV Alexander and Landau[17] have extended to proton scattering a microscopic, momentum space, optical potential theory which has been applied with some success to pion interactions with light nuclei.[18] Figure 7 illustrates their results along with our experimental data. The agreement for the differential cross section at large angles is encouraging, although overall quantitative agreement is only fair. It is significant that the theory employed is derived from first principles and contains no free parameters.

Dymarz and Malecki[19] have used an optical potential, derived from the Glauber model, in an exact solution of the Schrödinger equation. Their method accounts for centre of mass and short-range correlations and effectively includes all germs in the Glauber series. It is limited by present knowledge of the nucleon-nucleon parameters and omits possible exchange effects between the projectile and the target which might be important at large angles for some energies. A comparison of our data and the calculation at 350 MeV is shown in Fig. 8. It is interesting to speculate on how the calculation might be changed if spin-dependent amplitudes were to be included in the extraction of the potential.

An examination of Fig. 6 reveals that measurements near 275 MeV and 425 MeV could be useful in clearing up the energy-dependent behaviour of the analyzing power. As well, larger angle measurements of $d\sigma/d\Omega$ and $A_y(\theta)$ at and above 600 MeV would be welcome additional information.

Satisfactory tests of theoretical models of proton ^{4}He elastic scattering have been restricted by the limitations in available experimental data. The extensive measurements of $d\sigma/d\Omega$ and $A_y(\theta)$ provided by this experiment as well as those of Stetz *et al.*[1] and McCamis *et al.*[2] in the energy range of 200 to 500 MeV should aid in the resolution of this problem.

ACKNOWLEDGEMENTS

We would like to express our thanks to R. Abegg, A. Bishop, D.K. Hasell, D. Healey, and B.T. Murdoch who provided valuable assistance in the operation of the liquid helium target, and to H. Coombes who helped with the electronics during the experiment. This work was supported by the Natural Sciences and Engineering Research Council of Canada.

REFERENCES

*Present address: NIKHEF, Amsterdam, The Netherlands

[1]A.W. Stetz, J.M. Cameron, D.A. Hutcheon, R.H. McCamis, C.A. Miller, G.A. Moss, G. Roy, J.G. Rogers, C.A. Goulding, and W.T.H. van Oers, Nucl. Phys. A290, 285 (1977).

[2]R.H. McCamis, J.M. Cameron, L.G. Greeniaus, D.A. Hutcheon, C.A. Miller, G.A. Moss, G. Roy, M.S. de Jong, B.T. Murdoch, W.T.H. van Oers, J.G. Rogers, and A.W. Stetz, Nucl. Phys. A302, 388 (1978).

[3]L.G. Greeniaus, D.A. Hutcheon, C.A. Miller, G.A. Moss, G. Roy, R. Dubois, C. Amsler, B.K.S. Koene, and B.T. Murdoch, Nucl. Phys. A322, 308 (1979).

[4]C.A. Goulding, B.T. Murdoch, M.S. de Jong, W.T.H. van Oers, and R.H. McCamis, Nucl. Instr. and Meth. 148, 11 (1978).

[5]R.H. McCamis, Ph.D. thesis, University of Alberta (1977) unpublished.

[6]J.M. Cameron, P. Kitching, R.H. McCamis, C.A. Miller, G.A. Moss, J.G. Rogers, G. Roy, A.W. Stetz, C.A. Goulding, and W.T.H. van Oers, Nucl. Instr. and Meth. 143, 399 (1977).

[7]R. Klem, G. Igo, R. Talaga, A. Wriekat, H. Courant, K. Einsweiler, T. Joyce, H. Kagan, Y. Makdisi, M. Marshak, B. Mossberg, E. Peterson, K. Ruddick, and T. Walsh, Phys. Rev. Lett. 38, 1272 (1977).

[8]R. Klem, G. Igo, R. Talaga, A. Wriekat, H. Courant, K. Einsweiler, T. Joyce, H. Kagan, Y. Makdisi, M. Marshak, B. Mossberg, E. Peterson, K. Ruddick, and T. Walsh, Phys. Lett. 70B, 155 (1977).

[9]E. Aslanides, T. Bauer, R. Bertini, R. Beurtey, A. Boudard, F. Brochard, G. Bruge, A. Chaumeaux, H. Catz, J.M. Fontaine, R. Frascaria, D. Garreta, P. Gorodetzky, J. Guyot, F. Hibou, D. Legrand, M. Matoba, Y. Terrien, J. Thirion, and E. Lambert, Phys. Lett. 68B, 221 (1977).

[10]K. Gotow, University of Rochester report NYO-2532 (1959) unpublished.

[11]J. Bystricky and F. Lehar, in *Proceedings of the Fourth International Symposium on Polarization Phenomena in Nuclear Reactions*, Zürich, 1975 (Birkhauser, Basel, 1976), p. 458. We thank F. Lehar and C. Lechanoine for providing us with the most up-to-date predictions of the Saclay analysis.

[12]D.V. Bugg, J.A. Edgington, C. Amsler, R.C. Brown, C.J. Oram, K. Shakarchi, N.M. Stewart, G.A. Ludgate, A.S. Clough, D. Axen, S. Jaccard, and J. Va'vra, Jour. Phys. G. 7, 1025 (1978). We thank D.V. Bugg for providing us with their most up-to-date results.

[13]A. Houdayer, N.E. Davison, S.A. Elbakr, A.M. Sourkes, W.T.H. van Oers, and A.D. Bacher, Phys. Rev. C18, 1985 (1978).

[14]G.J. Igo, Rev. Mod. Phys. 50, 523 (1978).

[15]A.K. Kerman, H. McManus, and R.M. Thaler, Ann. Phys. (N.Y.) 8, 551 (1959).

[16]L.G. Arnold, B.C. Clark, and R.L. Mercer, Phys. Rev. C19, 917 (1979).

[17]Y. Alexander and R.H. Landau, Phys. Lett. 84B, 292 (1979).

[18]R.H. Landau, Phys. Rev. C15, 2127 (1977); R.H. Landau and A.W. Thomas, Nucl. Phys. A302, 461 (1978); R.H. Landau, S.C. Phatak, and F. Tabakin, Ann. Phys. 78, 299 (1973).

[19]R. Dymarz and A. Malecki, Phys. Lett. 66B, 413 (1977).

Table I. Properties of the system.

	Incident Proton Energy		
	200 MeV	350 MeV	500 MeV
Angular range covered (laboratory angle)			
Singles Mode	13° - 105°	15° - 91°	13° - 61°
Coincidence Mode	105° - 143°	91° - 143°	61° - 143°
Horizontal angular acceptance			
Singles Mode	2.14°	1.57°	1.40°
Coincidence Mode	3.48°	3.99°	2.33°
Solid angle acceptance[a]			
Singles Mode	1.55 msr	0.755 msr	0.600 msr
Coincidence Mode	3.27 msr	4.93 msr	1.816 msr
p-p analyzing power used for beam polarization	0.305	0.435	0.501

[a]Used in off-line analysis

Table II. Proton-^{4}He elastic scattering cross sections and analyzing power

θ_{lab} (deg)	$\frac{d\sigma}{d\Omega}_{lab}$ $\left(\frac{mb}{sr}\right)$	$-t\left(\frac{GeV}{c}\right)^2$	$\frac{d\sigma}{dt}\frac{mb}{\left(\frac{GeV}{c}\right)^2}$	Cross Section Error (%)	Analyzing Power	Error
T_p = 200 MeV						
4.7[a]	87.5	0.0028	663.	5.8		
6.3[a]	84.7	0.0050	643.	3.1		
7.9[a]	89.0	0.0079	677.	2.6		
9.5[a]	77.4	0.011	589.	2.3		
11.1[a]	64.8	0.016	495.	1.8		
12.8[a]	52.9	0.020	405.	1.6		
13.0	50.8	0.021	389.	0.8	0.816	0.015
14.4[a]	41.9	0.026	322.	1.5		
15.0	39.2	0.028	302.	1.0	0.899	0.018
17.0	30.0	0.036	232.	0.9	0.993	0.019
19.0	23.1	0.045	180.	0.9	1.008	0.021
21.0	17.2	0.054	135.2	1.0	1.003	0.022
23.0	13.1	0.065	103.2	1.0	0.883	0.021
25.0	9.73	0.076	77.5	1.0	0.752	0.021
27.0	7.82	0.088	62.8	1.1	0.583	0.019
29.0	6.23	0.101	50.5	1.1	0.390	0.019
31.0	4.81	0.114	39.4	1.0	0.208	0.018
33.0	3.93	0.128	32.5	1.1	-0.013	0.019
35.0	3.08	0.143	25.8	1.1	-0.184	0.020
37.0	2.38	0.158	20.1	1.1	-0.304	0.021
39.0	1.83	0.174	15.6	1.1	-0.455	0.019

TABLE II. *(Continued)*

θ_{lab} (deg)	$\frac{d\sigma}{d\Omega}_{lab}$ $\left(\frac{mb}{sr}\right)$	$-t\left(\frac{GeV}{c}\right)^2$	$\frac{d\sigma}{dt}\frac{mb}{\left(\frac{GeV}{c}\right)^2}$	Cross Section Error (%)	Analyzing Power	Error
41.0	1.44	0.191	12.4	1.1	-0.597	0.021
43.0	1.08	0.207	9.48	1.2	-0.680	0.022
45.0	0.782	0.225	6.95	1.3	-0.783	0.024
49.0	0.442	0.260	4.04	1.2	-0.927	0.027
53.0	0.249	0.297	2.35	1.5	-1.029	0.035
57.0	0.156	0.334	1.52	1.4	-0.957	0.030
61.0	0.102	0.372	1.02	1.6	-0.703	0.040
65.0	0.0791	0.410	0.826	2.5	-0.320	0.026
73.0	0.0559	0.486	0.628	1.9	-0.042	0.019
77.0	0.0473	0.523	0.553	1.9	0.025	0.018
80.0	0.0431	0.550	0.519	1.7	0.076	0.016
85.0	0.0348	0.594	0.440	1.5	0.118	0.015
90.0	0.0267	0.636	0.356	1.1	0.065	0.018
95.0	0.0196	0.676	0.275	1.5	-0.057	0.014
100.0	0.0142	0.714	0.210	1.5	-0.104	0.014
105.0	0.00934	0.750	0.145	1.5	-0.204	0.035
115.0	0.00400	0.813	0.0683	0.4	-0.592	0.012
125.0	0.00204	0.866	0.0381	0.8	-0.897	0.015
135.0	0.00158	0.909	0.0321	3.0	-0.632	0.017
140.0	0.00162	0.927	0.0340	0.9	-0.479	0.018
144.0[b]	0.00166	0.938	0.0358	1.4	-0.408	0.017
145.0	0.00165	0.943	0.0357	0.9	-0.358	0.017

TABLE II *(Continued)*

θ_{lab} (deg)	$\frac{d\sigma}{d\Omega}_{lab}$ $\left(\frac{mb}{sr}\right)$	$-t\left(\frac{GeV}{c}\right)^2$	$\frac{d\sigma}{dt}$ $\frac{mb}{\left(\frac{GeV}{c}\right)^2}$	Cross Section Error (%)	Analyzing Power	Error
152.0[b]	0.00176	0.961	0.0396	1.3	-0.385	0.014
158.0[b]	0.00170	0.973	0.0392	1.6	-0.375	0.020
163.0[b]	0.00164	0.981	0.0386	1.6	-0.359	0.020
168.0[b]	0.00152	0.987	0.0362	1.7	-0.305	0.022
T_p = 350 MeV						
3.9[a]		0.0036			0.265	0.027
4.6[a]	165.	0.0051	669.	3.3		
5.5[a]		0.0072			0.439	0.021
6.3[a]	122.	0.0093	494.	2.2		
7.1[a]		0.012			0.586	0.014
7.9[a]	99.9	0.015	405.	1.5		
8.8[a]		0.018			0.649	0.014
9.5[a]	82.8	0.021	337.	1.4		
10.4[a]		0.025			0.712	0.015
11.1[a]	68.6	0.029	280.	1.1		
12.0[a]		0.034			0.746	0.012
12.8[a]	54.8	0.038	224.	0.9		
13.7[a]		0.044			0.748	0.011
14.4[a]	42.7	0.048	175.5	0.9		
15.0	39.2	0.053	161.3	0.8	0.750	0.014

TABLE II. *(Continued)*

θ_{lab} (deg)	$\frac{d\sigma}{d\Omega}_{lab}$ $\left(\frac{mb}{sr}\right)$	$-t\left(\frac{GeV}{c}\right)^2$	$\frac{d\sigma}{dt}$ $\frac{mb}{\left(\frac{GeV}{c}\right)^2}$	Cross Section Error (%)	Analyzing Power	Error
15.3[a]		0.055			0.717	0.017
19.0	19.8	0.083	82.8	1.0	0.568	0.016
23.0	8.64	0.121	36.6	0.8	0.303	0.012
27.0	3.21	0.164	13.9	0.9	-0.082	0.012
31.0	0.972	0.213	4.28	1.0	-0.561	0.019
33.0	0.526	0.239	2.35	1.6	-0.822	0.026
35.0	0.300	0.266	1.36	1.4	-0.863	0.030
37.0	0.206	0.295	0.942	1.7	-0.614	0.026
39.0	0.164	0.324	0.760	1.8	-0.227	0.025
41.0	0.154	0.354	0.725	1.6	0.161	0.023
46.0	0.138	0.433	0.674	1.5	0.454	0.022
51.0	0.0941	0.516	0.479	1.6	0.374	0.025
56.0	0.0534	0.600	0.284	1.2	0.199	0.021
61.0	0.0278	0.686	0.155	1.0	0.023	0.013
66.0	0.0130	0.772	0.0761	2.3	-0.211	0.019
71.0	0.00688	0.857	0.0423	3.1	-0.465	0.028
76.0	0.00379	0.941	0.0245	3.4	-0.671	0.034
81.0	0.00240	1.02	0.0164	4.8	-0.802	0.053
86.0	0.00171	1.10	0.0123	6.0	-0.757	0.066
91.0	0.00121	1.17	0.00926	1.7	-0.713	0.015
96.0	9.88×10^{-4}	1.24	0.00796	1.6	-0.524	0.012
106.0	8.44×10^{-4}	1.37	0.00757	1.7	-0.139	0.013

TABLE II. *(Continued)*

θ_{lab} (deg)	$\frac{d\sigma}{d\Omega}_{lab}\left(\frac{mb}{sr}\right)$	$-t\left(\frac{GeV}{c}\right)^2$	$\frac{d\sigma}{dt}\frac{mb}{\left(\frac{GeV}{c}\right)^2}$	Cross Section Error (%)	Analyzing Power	Error
116.0	6.96×10^{-4}	1.48	0.00691	1.5	0.035	0.010
126.0	6.05×10^{-4}	1.57	0.00660	3.0	-0.085	0.011
136.0	4.97×10^{-4}	1.64	0.00590	1.2	-0.349	0.017
143.0	4.30×10^{-4}	1.68	0.00536	1.5	-0.552	0.024
146.0[b]	4.34×10^{-4}	1.70	0.00552	2.4	-0.695	0.029
152.0[b]	3.91×10^{-4}	1.72	0.00514	2.5	-0.744	0.028
157.0[b]	3.58×10^{-4}	1.74	0.00482	2.5	-0.791	0.028
163.0[b]	3.51×10^{-4}	1.76	0.00483	2.3	-0.763	0.030
168.0[b]	3.17×10^{-4}	1.77	0.00442	2.7	-0.547	0.032
T_p = 500 MeV						
3.9[a]		0.0055			0.283	0.018
4.7[a]	263.	0.0078	697.	2.4		
5.6[a]		0.011			0.386	0.015
6.3[a]	213.	0.014	566.	2 1		
7.2[a]		0.018			0.453	0.013
7.9[a]	163.	0.022	433.	1.4		
8.8[a]		0.028			0.530	0.012
9.5[a]	130.	0.033	348.	1.4		
10.4[a]		0.039			0.543	0.014
11.1[a]	93.7	0.044	251.	1.5		

TABLE II. *(Continued)*

θ_{lab} (deg)	$\frac{d\sigma}{d\Omega}_{lab}\left(\frac{mb}{sr}\right)$	$-t\left(\frac{GeV}{c}\right)^2$	$\frac{d\sigma}{dt}\frac{mb}{\left(\frac{GeV}{c}\right)^2}$	Cross Section Error (%)	Analyzing Power	Error
12.0[a]		0.051			0.565	0.013
12.7[a]	63.3	0.058	170.2	1.2		
13.0	61.0	0.060	164.2	0.9	0.508	0.020
13.6[a]		0.066			0.545	0.013
14.4[a]	42.9	0.074	115.9	1.1		
15.0	38.1	0.080	103.2	1.0	0.507	0.020
15.2[a]		0.082			0.488	0.017
17.0	21.7	0.102	59.1	1.0	0.403	0.019
19.0	11.2	0.127	30.7	0.9	0.314	0.015
21.0	5.52	0.154	15.3	0.9	0.164	0.015
23.0	2.40	0.184	6.72	0.9	-0.134	0.016
25.0	0.851	0.215	2.404	1.4	-0.452	0.026
27.0	0.350	0.249	0.998	1.6	-0.613	0.035
29.0	0.285	0.285	0.824	1.2	-0.076	0.026
31.0	0.330	0.323	0.963	0.9	0.397	0.018
33.0	0.351	0.362	1.039	1.0	0.503	0.017
35.0	0.341	0.404	1.023	1.0	0.488	0.018
37.0	0.308	0.446	0.939	0.9	0.468	0.018
39.0	0.256	0.490	0.792	1.0	0.374	0.017
41.0	0.196	0.535	0.615	1.0	0.345	0.018
46.0	0.805	0.653	0.263	1.1	0.162	0.019

TABLE II. *(Continued)*

θ_{lab} (deg)	$\frac{d\sigma}{d\Omega}_{lab}\left(\frac{mb}{sr}\right)$	$-t\left(\frac{GeV}{c}\right)^2$	$\frac{d\sigma}{dt}\frac{mb}{\left(\frac{GeV}{c}\right)^2}$	Cross Section Error (%)	Analyzing Power	Error
51.0	0.0260	0.776	0.0889	1.5	-0.078	0.025
56.0	0.00737	0.901	0.0265	2.2	-0.166	0.057
61.0	0.00228	1.03	0.00862	1.5	0.037	0.013
66.0	0.00141	1.15	0.00563	1.6	0.408	0.015
71.0	0.00111	1.28	0.00467	3.4	0.484	0.037
76.0	6.29×10^{-4}	1.40	0.00281	3.7	0.470	0.040
81.0	3.86×10^{-4}	1.52	0.00182	3.7	0.318	0.039
86.0	2.75×10^{-4}	1.63	0.00138	2.6	-0.026	0.026
91.0	2.44×10^{-4}	1.74	0.00130	2.9	-0.326	0.031
96.0	1.93×10^{-4}	1.84	0.00109	3.7	-0.561	0.042
101.0	1.97×10^{-4}	1.93	0.00117	3.6	-0.670	0.044
106.0	1.83×10^{-4}	2.02	0.00115	3.8	-0.677	0.047
116.0	1.49×10^{-4}	2.17	0.00105	4.7	-0.495	0.054
126.0	1.30×10^{-4}	2.30	0.00101	3.1	-0.144	0.058
136.0	1.45×10^{-4}	2.40	0.00123	4.8	-0.303	0.052
143.0	1.53×10^{-4}	2.46	0.00136	4.0	-0.482	0.051
145.0[b]	1.66×10^{-4}	2.47	0.00150	2.6	-0.531	0.024
151.0[b]	1.57×10^{-4}	2.51	0.00147	2.6	-0.580	0.036
154.0[b]	1.48×10^{-4}	2.53	0.00140	2.8	-0.625	0.034
160.0[b]	1.46×10^{-4}	2.55	0.00142	2.8	-0.695	0.046
165.0[b]		2.57			-0.578	0.035
168.0[b]	1.17×10^{-4}	2.58	0.00117	3.3	-0.482	0.047

[a] Data from Ref. 1 averaged over the same angular acceptance as this experiment.

[b] Data from Ref. 2. For 200 MeV the analyzing power of Ref. 2 has been adjusted by using 0.305 as the p-p analyzing power.

Figure captions

1. (a) Setup for the singles mode data. The thin counters (P) served as active collimators to reduce the number of protons scattered in the entrance or exit of the scattering chamber from being detected.
   (b) A schematic drawing of the target-detector arrangement for the coincidence mode measurements. The protons were detected in the rear telescopes and the ^{4}He recoils in the forward telescopes. The copper degraders were used to reduce the proton energies to 80-130 MeV at the entrance to the NaI detectors.

2. (a) A "worst case" spectrum in the NaI detector for singles data in the intermediate angle region at 500 MeV. The upper curve is the target full data before background subtraction. The lower curve is the net contribution from the helium alone. The arrows indicate the cuts defining the good events.
   (b) A typical spectrum showing the correlation between the proton energy and the ^{4}He dE/dx for the coincidence data. The clean separation from any background events is clear. The lines indicate the cuts placed on the data.

3. The differential cross section at 200, 350, and 500 MeV as a function of the four-momentum transfer -t. The data from Refs. 1 and 2 are included here. The normalization uncertainty is about 5% at all energies.

4. The p-^{4}He analyzing power as a function of $\theta_{c.m.}$ at 200, 350, and 500 MeV. The scale uncertainty is about 1-1.5% at all energies.

5. The magnitude of the analyzing power at the first maximum and at the first minimum as a function of incident proton energy.

6. An analyzing power contour diagram representing existing data between 130 and 1800 MeV.

7. The calculations of Ref. 17 along with a sample of the data of this experiment and that of (1) and (2).

8. The calculations of Ref. 19 along with a sample of the data of this experiment and that of (1) and (2).

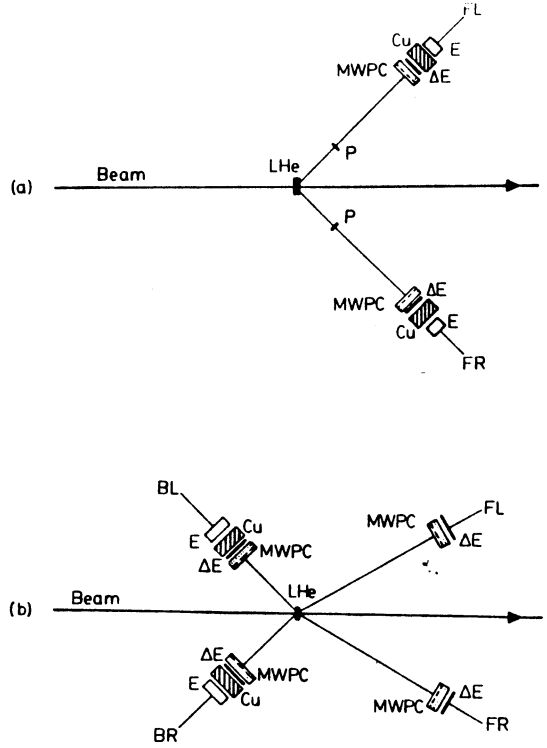

Fig. 1

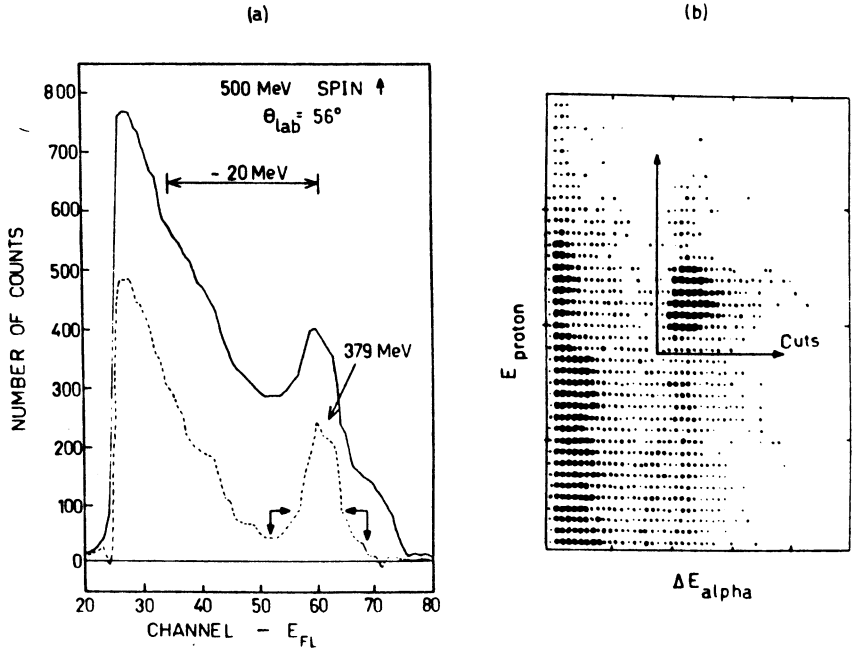

Fig. 2

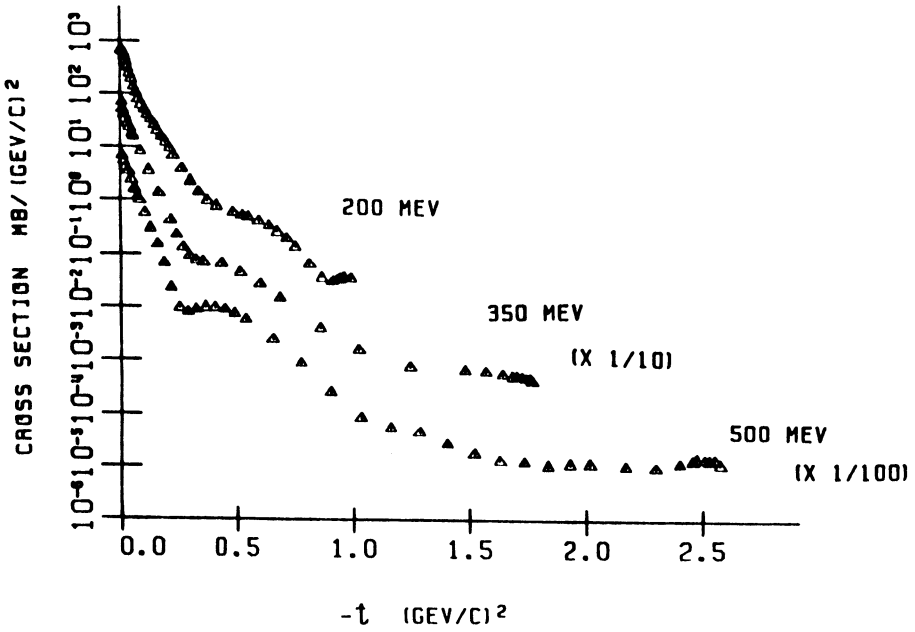

Fig. 3

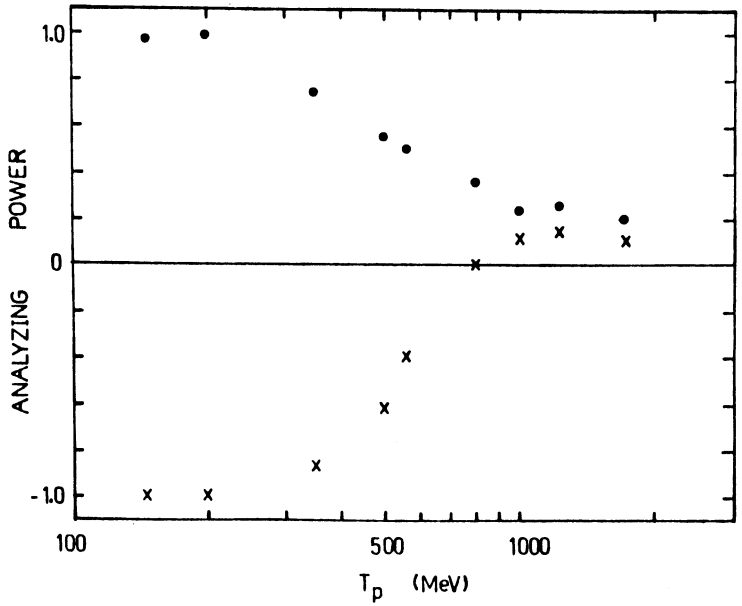

Fig. 5

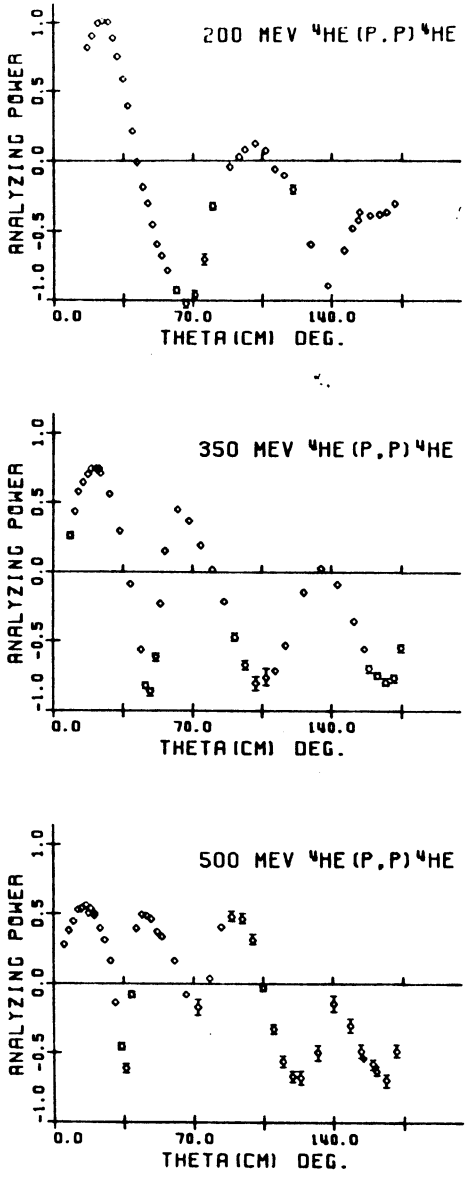

Fig. 4

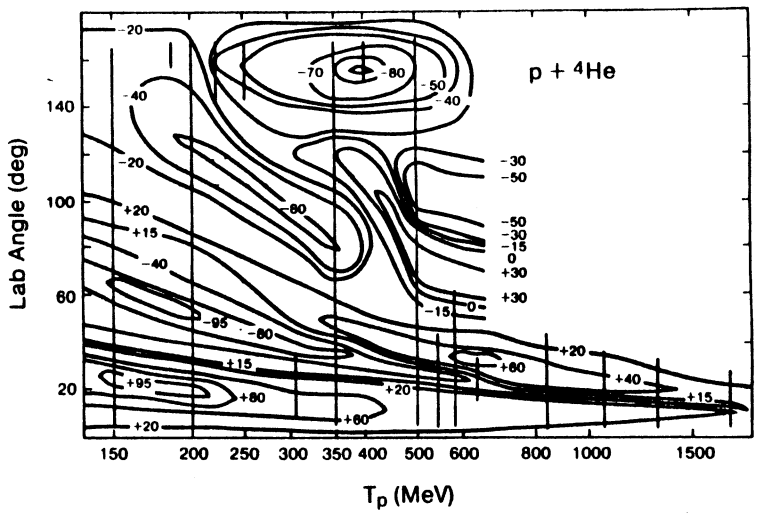

Fig. 6

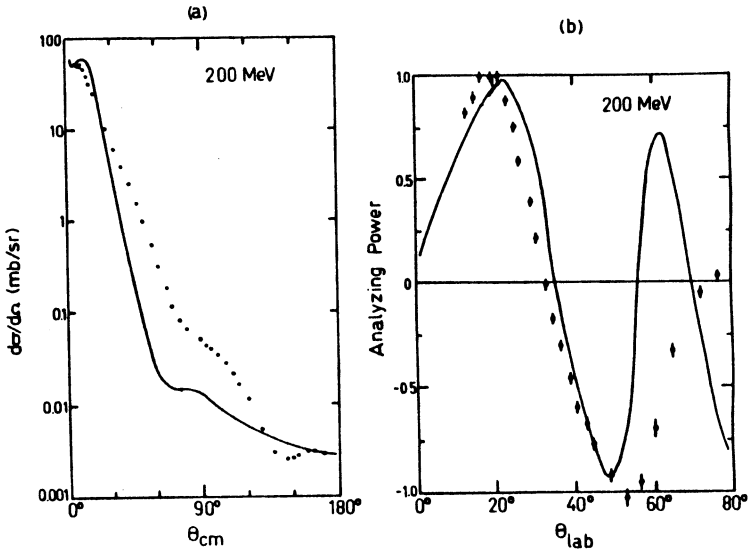

Fig. 7

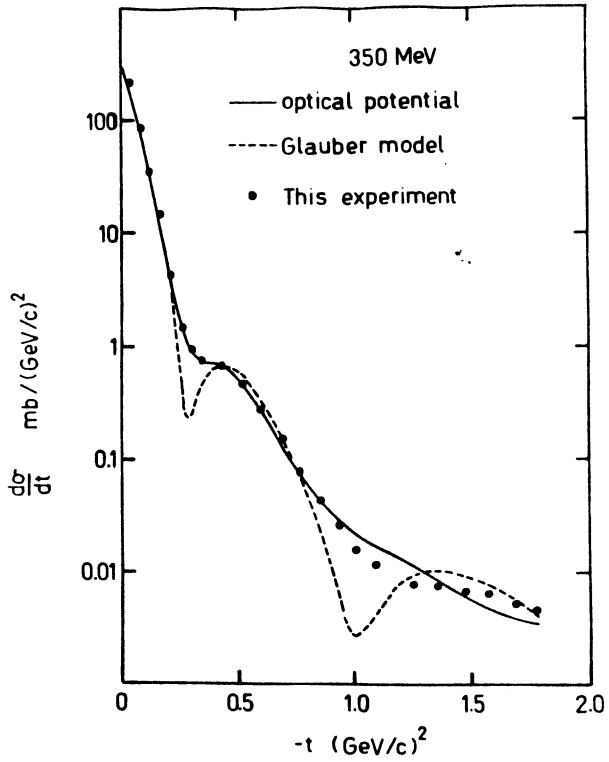

Fig. 8